Available online at www.sciencedirect.com
ScienceDirect
ELSEVIER
Journal of Catalysis 242 (2006) 287–298
JOURNAL OF CATALYSIS
www.elsevier.com/locate/jcat

Spatially resolved UV–vis microspectroscopy on the preparation of alumina-supported Co Fischer–Tropsch catalysts: Linking activity to Co distribution and speciation

Leon G.A. van de Water, G. Leendert Bezemer, Jaap A. Bergwerff, Marjan Versluijs-Helder, Bert M. Weckhuysen, Krijn P. de Jong *

Inorganic Chemistry and Catalysis, Department of Chemistry, Debye Institute, Utrecht University, Sorbonnelaan 16, 3508 TB Utrecht, The Netherlands

Received 30 March 2006; revised 1 June 2006; accepted 1 June 2006

Abstract

The preparation steps of Co/γ-Al_2O_3 Fischer–Tropsch (FT) catalysts have been studied using spatially resolved UV–vis microspectroscopy. The speciation of the different Co phases inside the support bodies changed by varying the composition of the impregnation solutions and the applied treatment, that is, subsequent impregnation, aging, drying, and calcination. The activity in the FT synthesis reaction of the reduced catalysts has been correlated with the applied preparation procedure. The highest activity was observed when γ-Al_2O_3 was impregnated with an aqueous $CoCO_3$ solution containing 1 equivalent citric acid. The formation of a Co citrate complex inside the support after impregnation was favored due to the higher pH of this solution compared with a similar solution involving $Co(NO_3)_2$. After calcination, Co_3O_4 was observed with an eggshell distribution, and no unfavorable $CoAl_2O_4$ was observed. The Co citrate complex formation is thought to restrict the extent of interaction of Co with alumina to form $CoAl_2O_4$, thereby allowing a higher degree of reduction and a concomitant higher catalytic activity. This study demonstrates the power of monitoring catalyst preparation with spatially resolved UV–vis microspectroscopy. The understanding of the physicochemical processes occurring at the different stages of the preparation process allows fine-tuning of the catalyst properties, which is ultimately expected to enable the development of improved supported catalysts.

Keywords: Supported catalysts; UV–vis spectroscopy; Catalyst preparation; Fischer–Tropsch; Co/γ-Al_2O_3

1. Introduction

In recent years, Fischer–Tropsch (FT) synthesis has attracted renewed interest as a result of stringent regulations on sulfur levels in transportation fuels and limited crude oil supplies. For decades, supported Co metal particles have been known to be very active for FT synthesis. Co-based FT catalysts are usually prepared by impregnation of a porous support, such as alumina, silica, titania, or, more recently, carbon, with a solution of a cobalt precursor salt [1–8]. Calcination results in conversion of the Co salt to oxidic species, which in the final step are converted into metallic Co by reduction in a hydrogen atmosphere. The catalytic performance is known to be a function of both the metal dispersion and the extent of reduction of the oxidic precursor species [9]. Both the dispersion of the Co and the reducibility of the oxidic precursor depend on the interaction of Co species with the support; a weak Co–support interaction is favorable for the reduction step, but may cause aggregation of the metal particles on reduction. When the Co–support interaction is strong, reaction between Co and the support may result in Co aluminate, titanate, or silicate species when Al_2O_3, TiO_2, or SiO_2 is used as the support. These Co–support species are generally not easily reduced, resulting in a decreased amount of metallic Co available for catalysis. The macrodistribution of Co metal over the support is another factor influencing catalytic performance. Packed-bed reactors, working under high pressures, require large (mm-sized) catalyst particles; restricted diffusion of CO into these catalyst particles decreases the reaction rate, and local high H_2/CO ratios may favor the formation

---

* Corresponding author. Fax: +31 30 2511027.
E-mail address: k.p.deJong@chem.uu.nl (K.P. de Jong).

0021-9517/$ – see front matter © 2006 Elsevier Inc. All rights reserved.
doi:10.1016/j.jcat.2006.06.004

of lighter products (low C_{5+} selectivity). These limitations can be overcome when Co is present only in the outer regions of the catalyst particles, that is, in a so-called "eggshell" distribution [10]. It is therefore evident that a delicate fine-tuning of the metal–support interactions during the different preparation steps is essential to obtain materials with optimal catalytic performance.

The aim of this study is to investigate the metal ion–support interactions throughout the preparation process of alumina-supported Co FT catalysts. We have chosen to study catalysts supported on mm-sized metal oxide bodies because this is the preferred type of support used in industrial processes with fixed-bed reactors [10]. In a previous study, the preparation process of CoMo/γ-Al_2O_3 catalyst bodies was monitored by combined time and spatially resolved UV–vis and Raman microspectroscopy [11,12]. The role of the different synthesis parameters in the formation and subsequent decomposition of a Co- and Mo-containing heteropolyanion inside γ-Al_2O_3 pellets could be successfully identified in this way.

In the present study, spatially resolved UV–vis microspectroscopy [13] was applied to monitor the Co oxide speciation and distribution during all steps of supported catalyst preparation. We show that the choice of the Co precursor, the impregnation solvent, the presence of additional ligands, and the applied drying/calcination procedure all had significant effects on the final Co speciation, the Co distribution throughout the Al_2O_3 support bodies, and, consequently, the catalytic performance of the different catalysts in the FT synthesis.

2. Experimental

2.1. Catalyst preparation

All samples were prepared by pore-volume impregnation of γ-Al_2O_3 pellets with metal-salt solutions. Cylindrical γ-Al_2O_3 pellets (Engelhard, 3 mm in both length and diameter), which were calcined at 600 °C for 6 h and stored at 120 °C, were applied. The pore volume of this support material was 1.0 ml/g, and its surface area was 200 m^2/g. The point of zero charge (pzc) of the γ-Al_2O_3 pellets was 8.9. The volume of the impregnated solutions was equal to the pore volume of the γ-Al_2O_3 sample plus 10%. Impregnated samples were kept in a closed vessel to prevent dehydration. All samples were aged for 5 min, dried in a preheated tubular oven in a dry oxygen-free nitrogen flow at 120 °C for 2 h, and finally heated in nitrogen at 550 °C (at a heating rate of 3 °C/min) for 3 h. These samples are referred to as calcined samples (c). Samples are labeled **x**(w), **x**(d), and **x**(c), where **x** refers to the impregnation solution used (see below) and (w), (d), and (c) refer to wet, dried, and calcined samples, respectively. Wet [**x**(w)] and dried [**x**(d)] samples taken for analysis were discarded after UV–vis measurements to ensure that the calcined samples [**x**(c)] were not exposed to air after the start of the drying and calcination steps.

Table 1
Metal solutions used for pore-volume impregnation experiments

	Metal precursor	Added ligand	Solvent	$[Co^{2+}]$ (M)	pH	*d* (g/ml)
1	$Co(NO_3)_2$	–	Water	1.35	3.2	1.19
2	$Co(NO_3)_2$	–	EtOH anh.	1.35	–	1.02
3	$Co(NO_3)_2$	1 eq. citric acid	Water	1.35	0.3	1.28
4	$Co(NO_3)_2$	1 eq. citric acid	EtOH anh.	1.35	–	1.12
5	$CoCO_3$	1 eq. citric acid	Water	1.35	3.1	1.20
6	$CoCO_3$	7.3 eq. NH_3	Water	1.35	10.3	1.16

Table 2
Co^{2+} absorption maxima in the UV–vis spectra of the impregnation solutions

	Transition [11]	λ (nm)
1	$^4T_{1g} \rightarrow {}^4T_{1g}$ (P)	511
2	$^4T_{1g} \rightarrow {}^4T_{1g}$ (P)	519
3	$^4T_{1g} \rightarrow {}^4T_{1g}$ (P)	511
4	$^4T_{1g} \rightarrow {}^4T_{1g}$ (P)	517
5	$^4T_{1g} \rightarrow {}^4T_{1g}$ (P)	511
6	$^4T_{1g} \rightarrow {}^4T_{1g}$ (P)	513

The Co concentration in all impregnation solutions was 1.35 M, corresponding to a metal content of 8.0 wt% after reduction. This amount of metal contained within the samples was chosen because it is a compromise between obtaining good spectroscopic data, which is limited by high metal loadings, and relevant FT catalysis, which is usually performed over catalysts with Co content >10 wt% [1]. The compositions of the impregnation solutions and the main absorption band in the visible part of the UV–vis spectra [14] are summarized in Tables 1 and 2, respectively. Dry EtOH (Merck, p.a.) was obtained by distillation from Mg and stored over 4-Å molecular sieves. A water-free solution of $Co(NO_3)_2$ in dry EtOH (**2**) was obtained by reacting 3.93 g (13.5 mmol) of $Co(NO_3)_2{\cdot}6H_2O$ (Acros, p.a.) with 4.40 g (29.7 mmol) of ethyl orthoformate (Acros, p.a.) to remove crystal water. Excess ethyl orthoformate and EtOH, formed on reaction, were then removed under reduced pressure. The deep-purple anhydrous $Co(NO_3)_2$ crystals thus obtained were redissolved in dry EtOH in a dry nitrogen atmosphere to a total volume of 10 ml (1.35 M Co). Solution **4** was prepared in the same manner, with citric acid (OPG Pharma, p.a.) added to the $Co(NO_3)_2{\cdot}6H_2O$ before reaction with ethyl orthoformate. Aqueous solutions containing citric acid as additional ligand (**3** and **5**) were prepared by dissolving the appropriate amount of citric acid in water before adding the Co salt [$Co(NO_3)_2$ and $CoCO_3$ (Acros, p.a.), respectively]. Basic solution **6** was prepared as described in the patent literature [15]; 25.4 g (264 mmol) of $(NH_4)_2CO_3$ (Acros, p.a.) was dissolved in 100 ml of a 25 wt% ammonia solution (Merck, p.a.) under gentle heating. Then 21.1 g (177.6 mmol) of $CoCO_3$ was slowly added, and the mixture was stirred for 2 h at 40–45 °C. The solution was finally filtered over a cellulose filter and stored under a nitrogen atmosphere to prevent air oxidation.

2.2. Characterization techniques

2.2.1. UV–vis

UV–vis (DRS) spectra were recorded (i) on wet impregnated Al_2O_3 support bodies after 5 min of aging, (ii) after 2 h drying at 120 °C, and (iii) after 3 h of calcination at 550 °C. All UV–vis measurements were performed using a previously described custom-made setup [13]. Spectra were recorded across a line through the middle of the cross-section of pellets that were bisected (using a razor blade) in the middle, perpendicular to their axis. The spatial resolution of these measurements was around 100 µm, and 10–15 spectra were recorded along each cross-section, requiring approximately 3 min. Powder X-ray diffraction (XRD) measurements were recorded on a CPS120 XRD system with a curved position-sensitive INEL detector (Bruker AXS, Delft, The Netherlands), and applying a Co$K\alpha$ radiation source ($\lambda = 1.788965$ Å). EDX line scans were obtained with an XL30SFEG (FEI, The Netherlands) scanning electron microscope. Analysis of the spectra was done with EDAX software (Tilburg, The Netherlands). The estimated relative error in the measurements depended on the absolute Co concentration and was found to be in the range of 5% (local Co content >5 wt%) to 30% (local Co content <1 wt%).

Table 3
Spectral assignments of the different phases, including the related references

Co phase	Transition	λ (nm)	Reference
$Co(OH_2)_6^{2+}$ (O_h)	$^4T_{1g} \rightarrow {}^4T_{1g}$ (P)	515	[14]
	$^4T_{1g} \rightarrow {}^4A_{2g}$	625	[14]
$Co(OH_2)_5(OH_s)^{2+}$ (O_h)	$^4T_{1g} \rightarrow {}^4T_{1g}$ (P)	535	[18]
	$^4T_{1g} \rightarrow {}^4A_{2g}$	635	[18]
Co^{II}–Al HT[a] (O_h)	$^4T_{1g} \rightarrow {}^4T_{1g}$ (P)	525	[21], this work
	$^4T_{1g} \rightarrow {}^4A_{2g}$	640	[21], this work
Co^{III}–Al HT[a] (O_h)	$^1A_{1g} \rightarrow {}^1T_{2g}$	380	[25,26], this work
	$^1A_{1g} \rightarrow {}^1T_{1g}$	650	[25,26], this work
$CoAl_2O_4$ (T_h)	$^4A_2 \rightarrow {}^4T_1$ (P)	545	[14,27]
	$^4A_2 \rightarrow {}^4T_1$ (P)	580	[14,27]
	$^4A_2 \rightarrow {}^4T_1$ (P)	630	[14,27]
Co_3O_4 (Co^{3+} (O_h))	$^1A_{1g} \rightarrow {}^1T_{2g}$	380	[27,28]
	$^1A_{1g} \rightarrow {}^1T_{1g}$	700	[27,28]
NO_3^-	$n \rightarrow \pi^*$	300	[14,16,17]

[a] Co–Al hydrotalcite, with general formula $[Co_{(1-x)}Al_x(OH)_2^{x+}]A_{x/n}^{n-}$, where A is the counter anion.

2.3. Fischer–Tropsch synthesis

FT synthesis (FTS) was performed using a custom-built set-up. In each case, two intact Co-loaded Al_2O_3 pellets (∼50 mg) were mixed with SiC (0.2 mm) and were reduced in a flow of hydrogen (20 ml/min) in He (40 ml/min). The sample was heated at a rate of 5 °C/min to a final temperature of 350 °C, where it was maintained for 2 h. The sample was then cooled to 220 °C, and FT synthesis was performed in a H_2/CO flow (2:1 volume ratio), with the flow adjusted in such a way that the conversion was 2.0% with a margin of 0.05%. The final activity and selectivity were measured after steady-state conditions were reached, typically after 20 h. FTS was performed at 1 bar total pressure, with partial pressures of the products (hydrocarbons and water) of approximately 2% and partial pressures of CO and H_2 of approximately 33 and 65%, respectively.

3. Results and discussion

3.1. UV–vis microspectroscopy

The impregnation of γ-Al_2O_3 pellets with $Co(NO_3)_2$ was performed with both aqueous solution **1** and EtOH solution **2**. The UV–vis spectra recorded across the cross-sectional surface of bisected pellets after 5 min of aging, after drying, and after calcination are depicted in Fig. 1. The assignments of the absorption bands recorded on the wet, dried, and calcined samples are summarized in Table 3. Images of the corresponding bisected dried and calcined samples are depicted in Fig. 2. In the spectra of both wet samples **1**(w) and **2**(w) (Fig. 1), an asymmetric band centered around 516 nm, indicative of O-donor octahedral Co^{2+} complexes [$^4T_{1g} \rightarrow {}^4T_{1g}$ (P) transition], is clearly discernible. The intense band at 296 nm is due to the NO_3^- $n \rightarrow \pi^*$ charge-transfer band [14,16,17]. The slower migration rate of Co^{2+} toward the core of the pellets in EtOH-containing sample **2**(w) compared with sample **1**(w), which was impregnated with the aqueous solution, is clearly visible. The slower migration rate may be due to the presence of bulky $[Co(EtOH)_6]^{2+}$ complexes instead of hydrated Co^{2+} ions, which could also explain the small difference in the observed main UV–vis absorption bands of solutions **1** and **2** (Table 2). The spectra of the dried samples [Fig. 1, **1**(d) and **2**(d)] also show that there is still very little Co in the core of the pellets of sample **2**(d). On drying, slight changes in the spectra of sample **1** (i.e., the appearance of an additional shoulder at around 635 nm) are observed. This band has been investigated in great detail [18,19] and has been shown to originate from Co^{2+}-surface complexes, formed by displacement of some of the water ligands around Co^{2+} by bridging surface hydroxyl groups. The spectral changes for sample **2** on drying are more pronounced; the 516-nm band in the spectra of **2**(w) disappears in favor of (near the edge of the bisected pellet) bands at 650 nm (with a shoulder at higher wavelength) and 380 nm. The spectra recorded more toward the core of the pellet display a band at 525 nm with a shoulder at 640 nm, along with a strong absorption band in the 350–400 nm region. The photograph of bisected pellet **2**(d) in Fig. 2 shows that the different regions in this sample have marked color differences, that is, brown near the edge and pink toward the center of the pellet. However, immediately after removal from the inert nitrogen atmosphere in the drying oven, the sample was still completely pink. The brown color near the edge of the pellets appeared within a few minutes after exposure to air, pointing to the presence of a Co^{2+} species that is easily oxidized. One possibility is Co–Al hydrotalcite (HT, with the general formula $[M_{(1-x)}^{2+}M_x^{3+}(OH)_2^{x+}]A_{x/n}^{n-}\cdot mH_2O$), which is known to be formed on metal-ion-assisted alumina dissolution [20]. Oxidation of Co^{2+} to Co^{3+} in such an HT structure has been reported in a study on Co–Al HTs with various Co^{2+}:Al^{3+} ratios. Samples with a Co^{2+}:Al^{3+} ratio of 5 were reported to be brown (due to the presence of Co^{3+}), whereas samples with lower Co^{2+}:Al^{3+} ratios were pink [21]. X-ray absorption spectroscopy (XANES) was used to prove that oxidation of around 30% of the Co^{2+} in the sample with a Co^{2+}:Al^{3+} ratio of 5 had occurred [21]. To verify that Co–Al HT had formed on drying of **2**, a Co–Al HT reference material with a Co^{2+}:Al^{3+} ratio of 3 and CO_3^{2-} as the anion was prepared as described previously [22]. The powder XRD pattern of the pink product (Fig. 3) agrees well with that of Co–Al

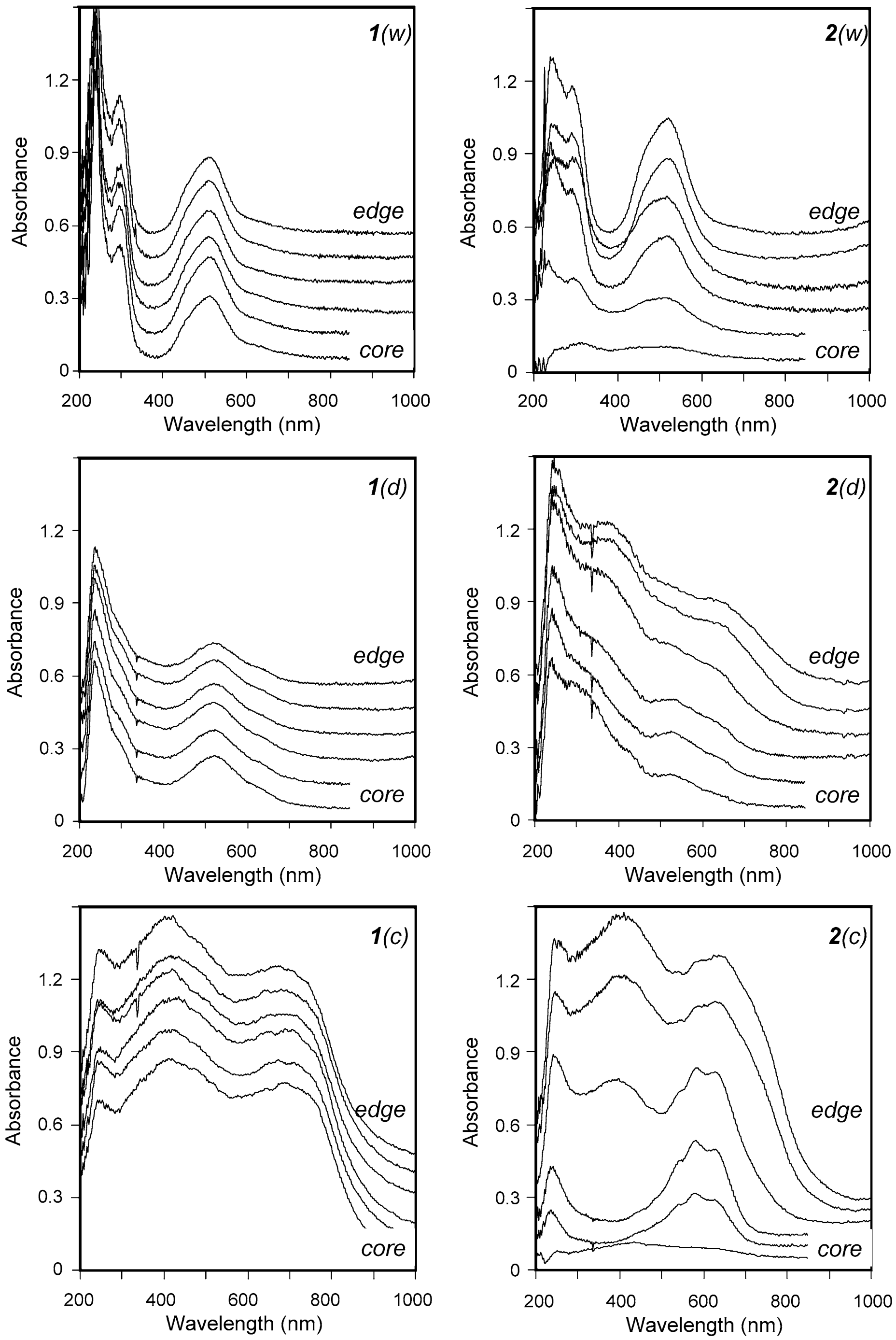

Fig. 1. UV–vis spectra recorded on bisected pellets, from edge to core, measured 5 min after impregnation (**1**(w) and **2**(w)), after drying at 120 °C (**1**(d) and **2**(d)) and after calcination at 550 °C (**1**(c) and **2**(c)).

HT reported in the literature [23,24]. The color of the material changed from pink to light brown overnight on exposure to air; the UV–vis spectra of both samples are depicted in Fig. 4 [traces (a) and (b), respectively]. The XRD pattern of the sample does not change on exposure to air, suggesting that the HT structure is conserved on oxidation. The main feature in the UV–vis spectrum of the pink reference sample is a band at around 525 nm, with a shoulder at 640 nm. An additional band at 350–400 nm is observed in the spectrum of the brown sample, which clearly resembles that of the brown area of sample **2**(d) [trace (c) in Fig. 4]. On the basis of the above, the absorption band of **2**(d) in the 350–400 nm region is assigned to octahedral Co^{3+} (HT) ($^1A_{1g} \rightarrow {}^1T_{2g}$ transition), in agreement with the literature [25,26]. The band around 650 nm near the edge of the pellets is also assigned to Co^{3+} (O_h) ($^1A_{1g} \rightarrow {}^1T_{1g}$ transition) [26]. The extended oxidation of Co^{2+} near the edge of the pellets on exposure to air agrees well with the assumption that a sufficiently high local Co:Al ratio is necessary for oxidation [21]. The spectra of **2**(w) before drying suggest that there indeed is a clear concentration gradient over sample **2**. The band

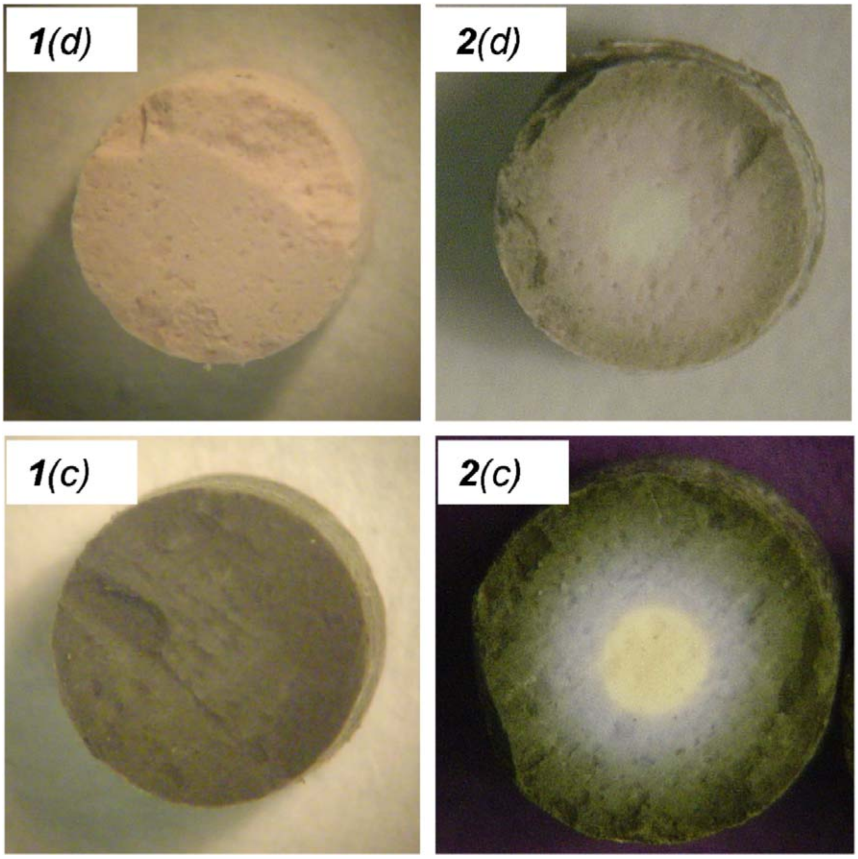

Fig. 2. Pictures of dried bisected pellets **1**(d) and **2**(d), and of bisected calcined samples **1**(c) and **2**(c).

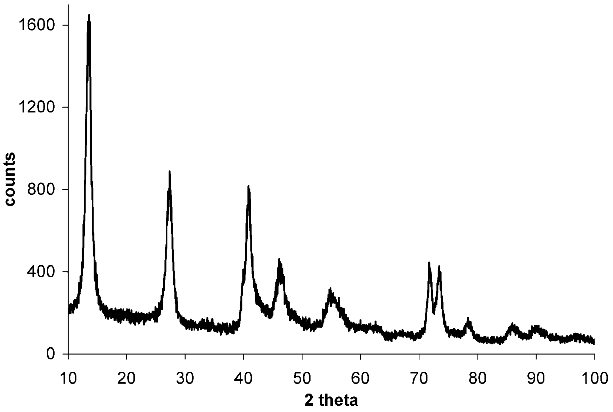

Fig. 3. X-ray diffraction pattern of a Co–Al HT reference sample with a Co:Al ratio of 3.

at 525 nm, still prominent in the pink region near the core of the pellets, is due to octahedral Co^{2+} (HT). The 640-nm band in the same region is assigned to Co^{2+}–surface complexes, similar to the assignment of this band in the case of **1**(d). HT formation calls for substantial amounts of water to react with the Co precursor and the Al_2O_3 support. Because HT formation is observed in **2**(d) with no water present in the (ethanolic) impregnation solution, water is thought to enter the sample while the (previously calcined and dried) γ-Al_2O_3 pellets are being weighed. Alternatively, water also may be provided by the Al_2O_3 surface, because the typical hydroxyl concentration of 5 OH/nm^2 is sufficient to account for the observed HT formation.

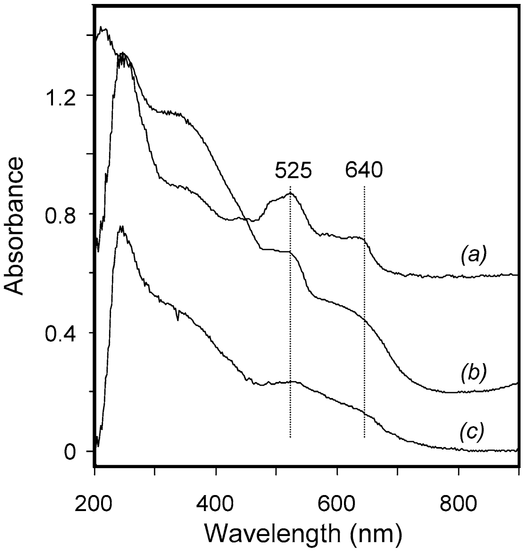

Fig. 4. UV–vis spectra of Co–Al HT (a) freshly prepared (pink), (b) after aging (light brown), as compared to a spectrum from sample **2**(d) (recorded 0.7 mm from core) taken from Fig. 1 (trace (c)).

The UV–vis spectra of calcined sample **1**(c) (Fig. 1) show the presence of Co_3O_4 throughout the whole sample, as evidenced by strong absorptions at 410 and 700 nm due to Co^{3+} in octahedral positions [25,27–29]. Similar to **2**(d), three dif-

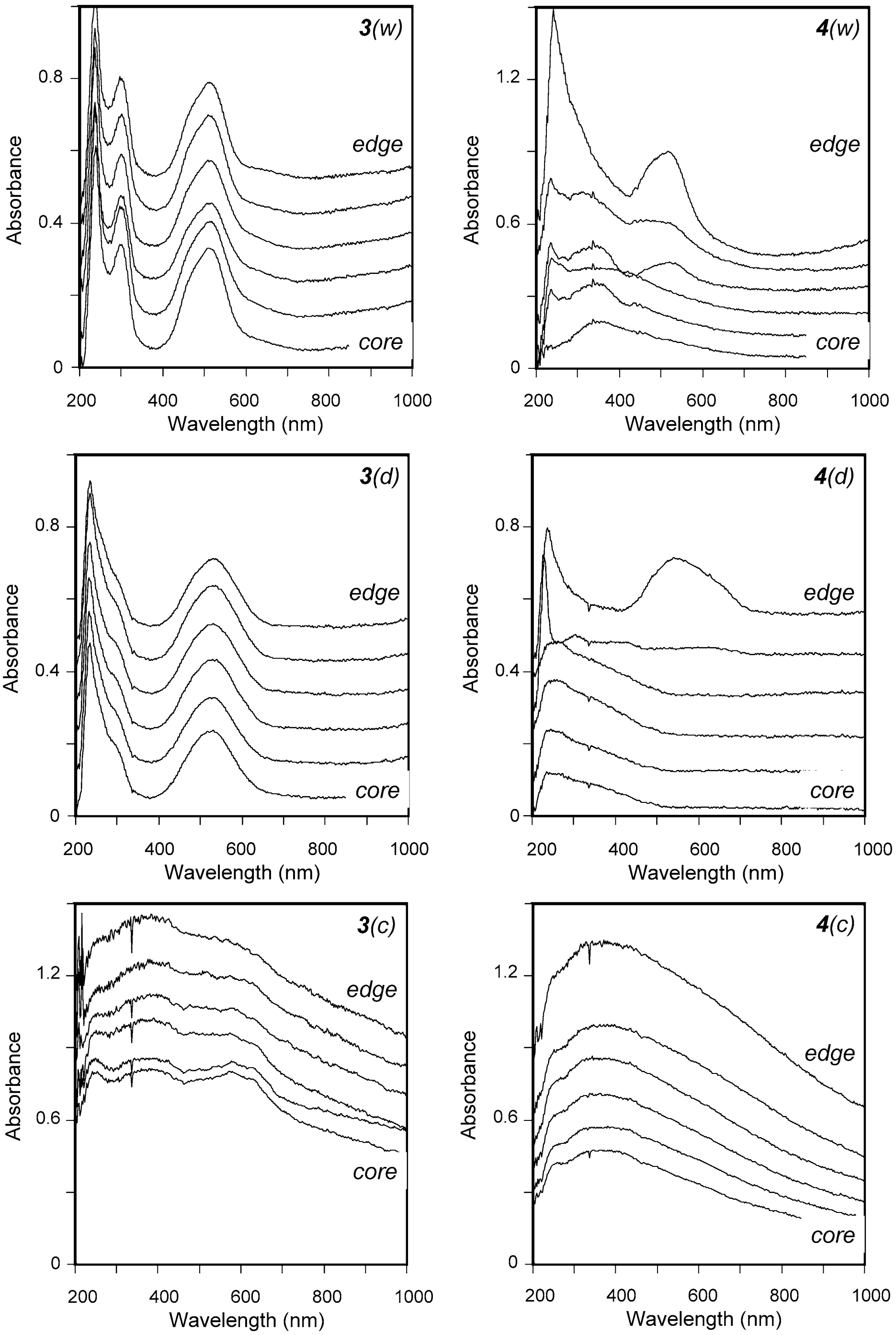

Fig. 5. UV–vis spectra recorded on bisected pellets, from edge to core, measured 5 min after impregnation (**3**(w) and **4**(w)), after drying at 120 °C (**3**(d) and **4**(d)) and after calcination at 550 °C (**3**(c) and **4**(c)).

ferent regions can be identified for sample **2**(c): a black outer ring, a blue inner ring, and a white core (see Fig. 2). The spectra recorded near the edge of the cross-section of bisected **2**(c) pellets are slightly different from the **1**(c) spectra, with absorption maxima at around 400 and 650 nm for **2**(c), due to the presence of Co_3O_4. The spectra corresponding to the blue region in the pellet feature a well-defined triplet at 540, 580, and 630 nm corresponding to Co^{2+} ions in a tetrahedral environment [$^4A_2 \rightarrow {}^4T_1$ (P) transition] [14,27]. This Co aluminate is the barely reducible $CoAl_2O_4$ (spinel), which is formed on migration of Co^{2+} ions into tetrahedral sites of the γ-Al_2O_3 lattice [18,27,28,30]. As in the previously discussed samples impregnated with EtOH solution **2**, hardly any Co is observed in the core of this sample. From both the spectra in Fig. 1 and the pictures in Fig. 2, it is clear that $CoAl_2O_4$ has evolved on calcination from Co^{2+}–Al HT in sample **2**(d), that is, in places where no oxidation of Co^{2+} occurred at the drying stage. Co_3O_4 is observed in those places where oxidation of Co^{2+} was observed on drying. Alternatively, the observed Co_3O_4 and $CoAl_2O_4$ regions may also be explained by the Co concentration gra-

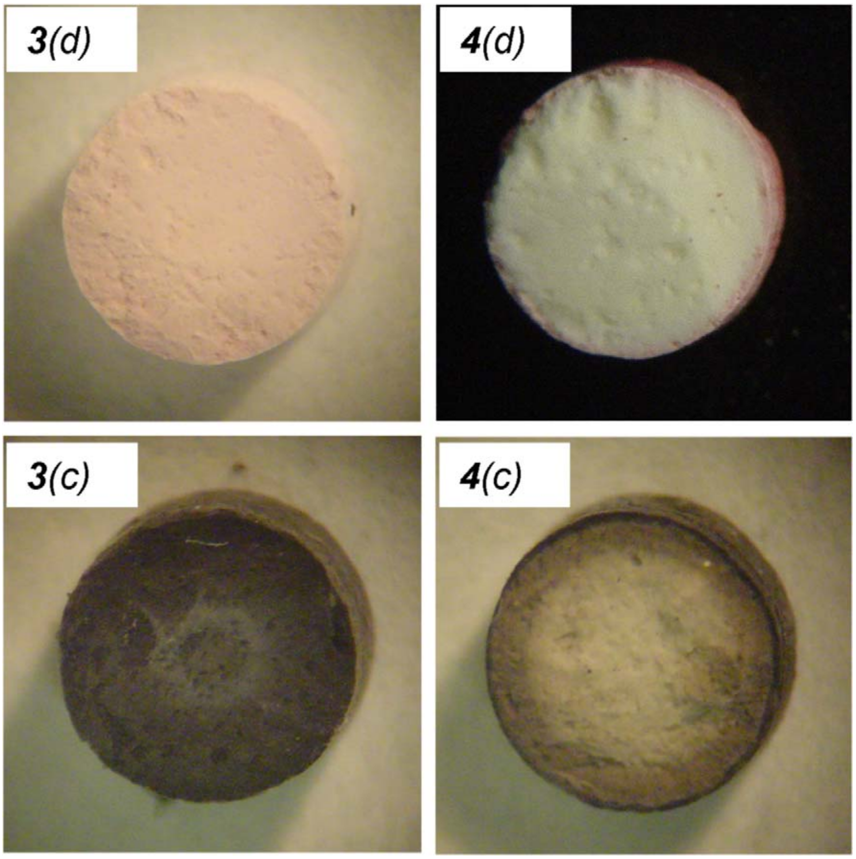

Fig. 6. Pictures of dried bisected pellets **3**(d) and **4**(d), and of bisected calcined samples **3**(c) and **4**(c).

dient over sample **2**. Low Co concentrations (in other words, low Co:Al ratios) may favor mixed metal–support species (i.e., $CoAl_2O_4$), whereas in regions with higher Co concentrations, the pure metal oxide (Co_3O_4) is the predominant species. The lack of a Co concentration gradient over sample **1** explains the absence of $CoAl_2O_4$ in **1**(c). A similar influence of the Co concentration on the species formed after calcination was reported by Liotta et al., who found $CoAl_2O_4$ in a 1-wt% Co–Al_2O_3 sample after calcination at 500 °C and Co_3O_4 after calcination of a 3 wt% sample [27], and by Ataloglou et al., who reported similar results for a range of Co–Al_2O_3 samples with varying Co concentrations [16]. Finally, the dispersion of the Co oxide phase that emerges on calcination is expected to play a role in $CoAl_2O_4$ formation in **2**(c). Calcination of the Co–Al HT phase [sample **2**(d)] may result in highly dispersed CoO, which easily reacts with the support to form $CoAl_2O_4$. In the case of **1**(c), in contrast, a low dispersion of Co_3O_4 is anticipated from $Co(NO_3)_2$ calcination [31], which does not give rise to the formation of $CoAl_2O_4$ in **1**(c).

The UV–vis spectra of γ-Al_2O_3 pellets impregnated with solutions **3** and **4** after 5 min of aging (w), after drying at 120 °C (d), and after calcination at 550 °C (c) are depicted in Fig. 5. The influence of the solvent on the migration rate is even more pronounced than in **1** and **2**. The EtOH solution of the Co–citric acid complex hardly enters the γ-Al_2O_3 pellets, as is also illustrated by the photographs taken after drying and calcination (Fig. 6), which is thought to be the result of the high viscosity of solution **4**.

Citrate ligands coordinate strongly to Co^{2+} at neutral pH (>4.5) [32], yielding an uncharged [Co(citrate)H] or negatively charged $[Co(citrate)]^-$ complex. At lower pH, the citrate ligands are not deprotonated and do not coordinate to the Co^{2+} ion, which exists as $[Co(OH_2)_6]^{2+}$. This is illustrated by the fact that the UV–vis spectra of aqueous $Co(NO_3)_2$ and Co(citrate) solutions (**1** and **3**) are identical. The Co speciation on impregnation and drying for sample **3** is similar to that of **1**, with the main absorption band due to Co^{2+} (O_h) at 514 nm [**3**(w)] and 527 nm [**3**(d)]. The 295-nm band is due to NO_3^- present in the sample [14]. However, a notable difference from the spectra of **1** is the absence of a band at 635 nm due Co^{2+}–surface interaction. The spectra of the calcined sample **3** show the presence of Co^{3+} (O_h) (at 375 and 640 nm), most likely as Co_3O_4, and, toward the core of the pellet, Co^{2+} (T_h) (at 545, 580, and 635 nm) in $CoAl_2O_4$, which is illustrated by the blue color in that region (Fig. 6). A Co concentration gradient may be the reason for the $CoAl_2O_4$ formation, in a similar fashion as in sample **2**(c). Co citrate solutions are known to be more viscous than Co nitrate solutions [33], which could decrease the migration rate of the complex into the core of the support pellets and thus cause a lower local Co concentration. $CoAl_2O_4$ surface spinel was not observed in sample **1**(c), where no citrate was present in the impregnation solution and no Co concentration gradient was

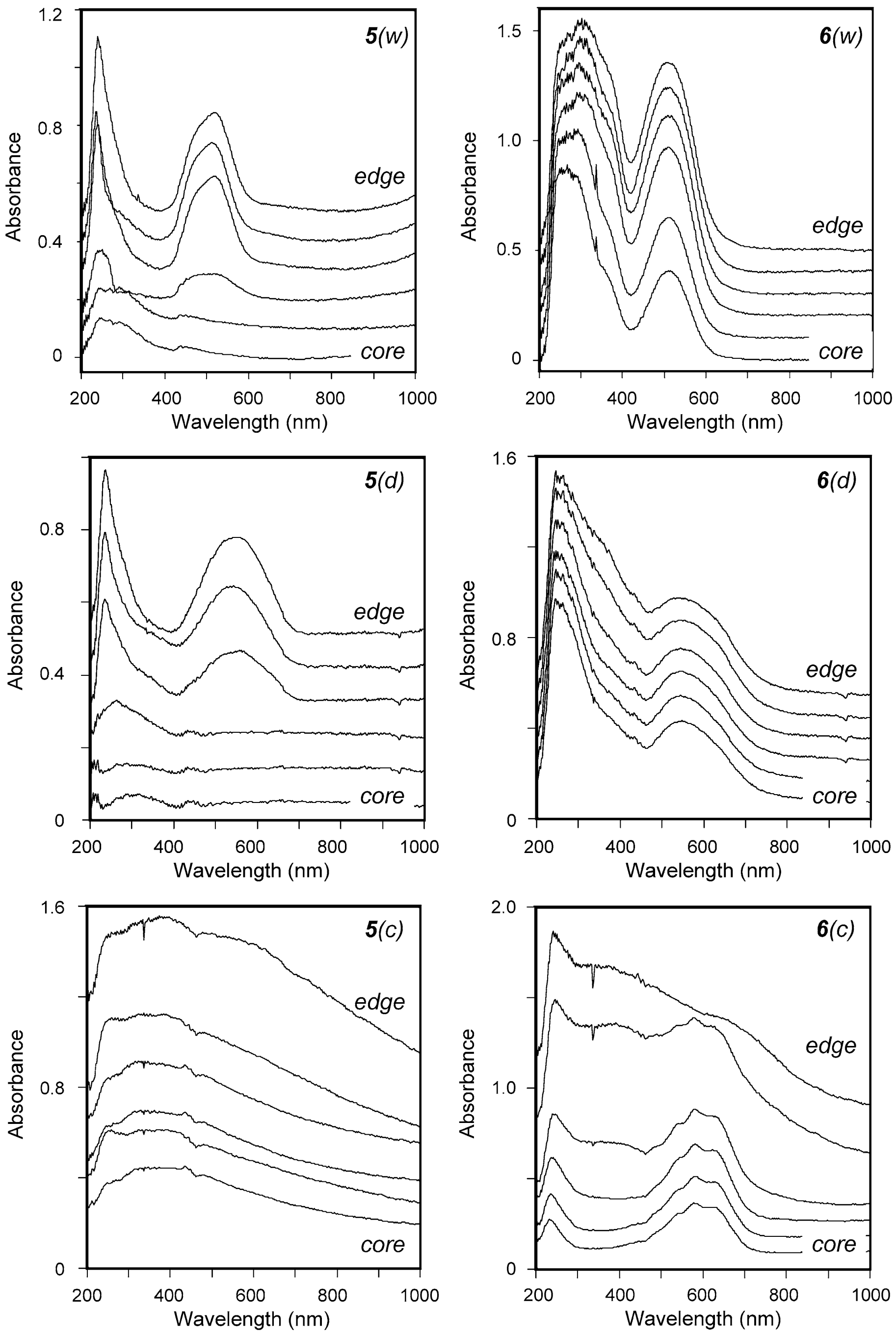

Fig. 7. UV–vis spectra recorded on bisected pellets, from edge to core, measured 5 min after impregnation (**5**(w) and **6**(w)), after drying at 120 °C (**5**(d) and **6**(d)) and after calcination at 550 °C (**5**(c) and **6**(c)).

observed. Alternatively, $CoAl_2O_4$ formation may result from a higher Co dispersion in **3**(d) compared with in **1**(d). Catalyst supports, impregnated with aqueous solutions of metal chelates, yield highly dispersed catalyst precursor species on drying, as redistribution of the metallic species is prevented by the high viscosity of the metal chelate solution [33]. Therefore, the metal dispersion after drying is expected to be higher in sample **3** than in sample **1**, and this highly dispersed Co reacts easily with the support to form $CoAl_2O_4$.

The spectra recorded on the wet sample impregnated with EtOH solution **4** shows the band at 516 nm of Co^{2+} (O_h) in the outer 0.1 mm of the cross-section, with no clear absorptions visible in the rest of the sample. After drying, the Co^{2+} (O_h) band is slightly red-shifted to 545 nm, and an additional broad shoulder around 370 nm is observed, which is tentatively assigned to Co^{3+} (O_h) ($^1A_{1g} \rightarrow {}^1T_{2g}$ transition). After calcination, no Co^{2+} (O_h) is visible; instead a very broad absorption band, which may be due to oxidized Co species, is observed throughout the entire sample, which points to Co migration at the calcination step. Comparing the photographs of **4**(d) and **4**(c) confirms that the thickness of the Co-containing area has increased on calcination.

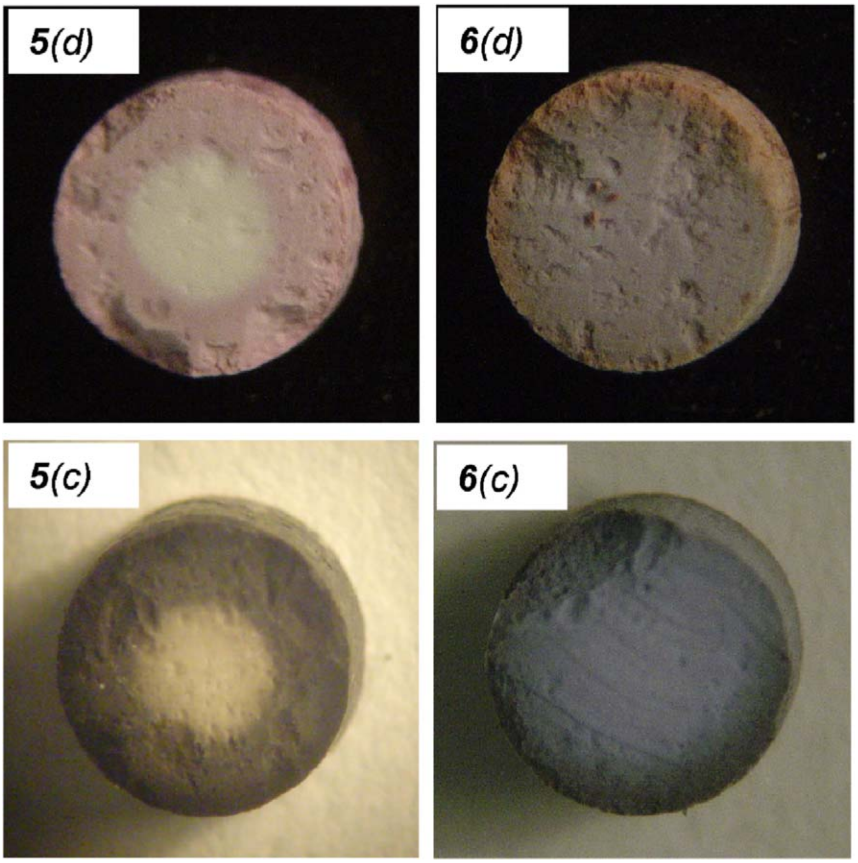

Fig. 8. Pictures of dried bisected pellets **5**(d) and **6**(d), and of bisected calcined samples **5**(c) and **6**(c).

The UV–vis spectra of Al_2O_3 pellets, impregnated with aqueous solutions **5** and **6**, are depicted in Fig. 7. The Co migration toward the core of the pellet is not complete after impregnation with $CoCO_3 +$ citric acid solution **5** after 5 min of aging. The Co concentration gradient is also clearly visible in the spectra of **5**(d) and **5**(c). The 517-nm band in sample **5**(w) is very similar to that found for **3**(w) (514 nm) and is indicative of the hydrated Co^{2+} (O_h) ion. After drying, the difference between samples **3** and **5** becomes more significant; the main Co^{2+} absorption band is observed at 527 nm for **3**(d) and at 550 nm for **5**(d). The difference may be due to the different pHs of the impregnation solution on replacement of NO_3^- for CO_3^{2-} counter ions; impregnation solution **5** has a pH of 3.1, and solution **3** has a pH of 0.3. Because of the higher pH, a larger fraction of the citric acid ligands are deprotonated and thus are able to form complexes with the Co^{2+} ions in **5**(d), causing a slight shift in the Co^{2+} (O_h) band. The Co citrate complexes thus formed may be either negatively charged (when all three carboxylic acid groups are deprotonated) or neutral (with two deprotonated carboxylic acid groups), and the Coulombic interaction with the protonated surface hydroxyl groups of the support will slow the Co transport. After calcination, there is still a clear difference between the spectra of **3**(c) and **5**(c). No $CoAl_2O_4$ is observed for **5**(c) as the triplet due to tetrahedral Co^{2+} (545, 580, and 635 nm) is absent in the spectra, even in those places where the local Co concentration is low. In contrast, the samples prepared from solutions **2** and **3** clearly contain this undesired spinel species after calcination. In the spectra of **5**(c) two broad bands at 375 and 640 nm, due to Co_3O_4, are visible in the outer region of the pellet, whereas a featureless absorption band is observed more toward the middle of the sample.

Sample **6**(w) shows a fairly homogeneous Co distribution throughout the sample, with a main absorption band at 512 nm that is identical to that of impregnation solution **6** (not shown). After drying, the main band is shifted to 545 nm. Calcined sample **6**(c) exhibits bands due to Co^{3+} in Co_3O_4 (400 and 690 nm) near the edge of the sample, along with three bands due to Co^{2+} (T_h) in the $CoAl_2O_4$ spinel (540, 580, and 635 nm); see Fig. 7. In Fig. 8, Co_3O_4 is shown as a dark ring near the edge of the sample, whereas the $CoAl_2O_4$ region is indicated by a blue color.

3.2. SEM-EDX

The UV–vis data discussed in the previous section provide spatially resolved information on the nature of Co oxide species in each sample. Rough indications on radial Co concentration gradients can also be obtained from these spectra, although quantification of these data is problematic in cases in which different species exist throughout the pellets and in which high metal-oxide loadings are used. The Co distribution was assessed in a more direct manner by SEM-EDX analysis. The Co profiles across bisected dried samples are shown in Fig. 9

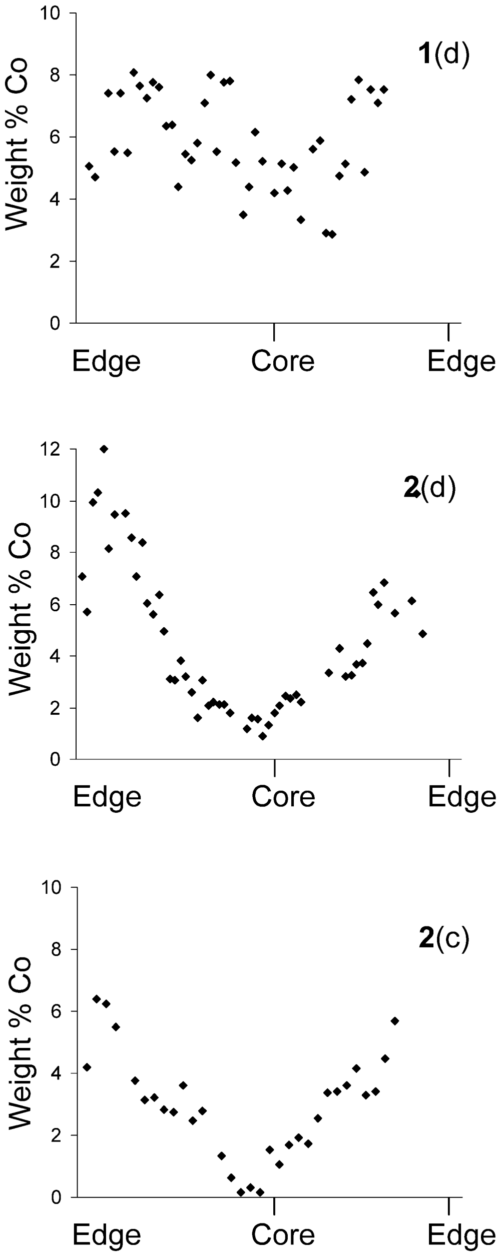

Fig. 9. Co distribution profiles over dried samples **1**(d) and **2**(d) and calcined sample **2**(c), as measured with SEM-EDX.

(**1** and **2**) and Fig. 10 (**3**–**6**). The profile of calcined sample **2**(c) is also presented in Fig. 9. The overall Co content of the samples seems to be somewhat lower than the expected value of 8 wt%, although the Co present near the very edge of the samples may not be accounted for completely due to the inherent limitations of the measurements. The measured Co profiles are in agreement with the UV–vis spectra; that is, a truly homogeneous Co distribution is found only in **1**, where samples **3** and **6** have only a moderate gradient. The Co concentration gradient over sample **2** is in agreement with the hypothesis used to explain the UV–vis spectra in the previous section; that is, air oxidation of Co^{2+} in the HT structure observed after drying occurs only at positions with high Co concentrations ($> \sim 3$ wt%).

Table 4
Co distribution and speciation of calcined samples, and catalytic performance of calcined and reduced samples measured at 1 bar, 220 °C, $H_2/CO = 2$ v/v, 2% CO conversion

	Distribution	Co_3O_4	$CoAl_2O_4$	Activity[a]	C_1 (wt%)	C_{5+} (wt%)	α[b]
1(c)	Uniform	++		1.6	15	58	0.74
2(c)	Egg-shell	+	+	0.3	20	42	0.68
3(c)	Intermediate	+	+	0.1	30	35	0.56
5(c)	Egg-shell	++		4.7	24	41	0.68
6(c)	Uniform		++	0.1	35	26	0.53

[a] Activity: 10^{-6} $\text{mol}_{CO}/(\text{s}\,\text{g}_{Co})$.
[b] α is the probability for chain growth derived from an Anderson–Schulz–Flory plot.

Similarly, after calcination, $CoAl_2O_4$ is observed only when the local cobalt concentration is $< \sim 3$ wt%, which agrees nicely with previously published findings [27]. The combination of the Co citrate complex and EtOH as the solvent prevents Co from entering the alumina pellet; the Co concentration is close to 0 wt% in **4**(d) (Fig. 10). When EtOH is replaced with water, a distribution close to homogeneous is observed [**3**(d); Fig. 10], although a gradient is still visible, and the observed $CoAl_2O_4$ in the UV–vis spectra of **3**(c) corresponds to local Co concentrations $< \sim 3$ wt%.

3.3. Fischer–Tropsch catalysis

The steady-state performance of the catalysts measured at 220 °C and 1 bar are reported in Table 4. Note that the spectroscopic data presented refer to calcined samples, whereas the catalytic data were obtained with calcined *and reduced* samples, where the Co distribution may be affected by the reduction step. Catalytic tests were performed with all calcined and reduced samples, except for **4**, because hardly any Co was present in these samples due to poor penetration of the Co citrate complex into the pores of the support. The Co-specific activity varied greatly, from 0.1 to 4.7×10^{-6} $\text{mol}_{CO}/(\text{s}\,\text{g}_{Co})$. The highest activity was observed for sample **5**, which was prepared using an aqueous solution of $CoCO_3$ and citric acid. The selectivity toward methane varied from 15 to 35 wt%, whereas the C_{5+} selectivity varied from 26 to 58 wt%. The highest selectivity toward C_{5+} was found for the catalyst prepared using $Co(NO_3)_2$ dissolved in water, containing poorly dispersed, homogeneously distributed Co_3O_4 particles after calcination. The chain growth probability ranged from 0.53 to 0.74 and nicely correlated with the trend in product selectivity.

The catalytic data show that calcined catalysts containing irreducible $CoAl_2O_4$ [**2**(c), **3**(c), and **6**(c)] exhibit lower activities than those without $CoAl_2O_4$ [**1**(c) and **5**(c)]. Differences between **1**(c) and **5**(c) are likely to be related to the larger Co surface area exposed by **5**(c), because it is known that aqueous impregnations with nitrate precursors may result in large particles [31,33]. The particle sizes of Co_3O_4 in **1**(c) and **5**(c) were analyzed by XRD; see Fig. 11. In the XRD pattern of **1**(c), peaks due to Co_3O_4 particles are visible, whereas in the case of **5**(c) no Co_3O_4 features can be seen, pointing to very small Co_3O_4 particles that cannot be detected by XRD.

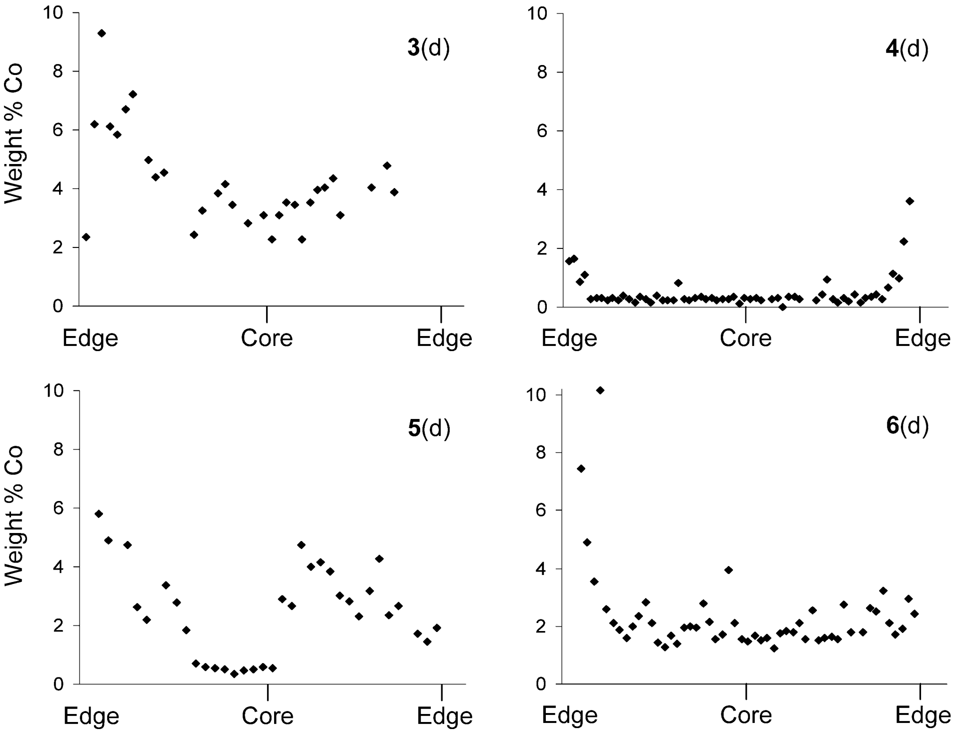

Fig. 10. Co distribution profiles over dried samples **3**(d), **4**(d), **5**(d), and **6**(d), as measured with SEM-EDX.

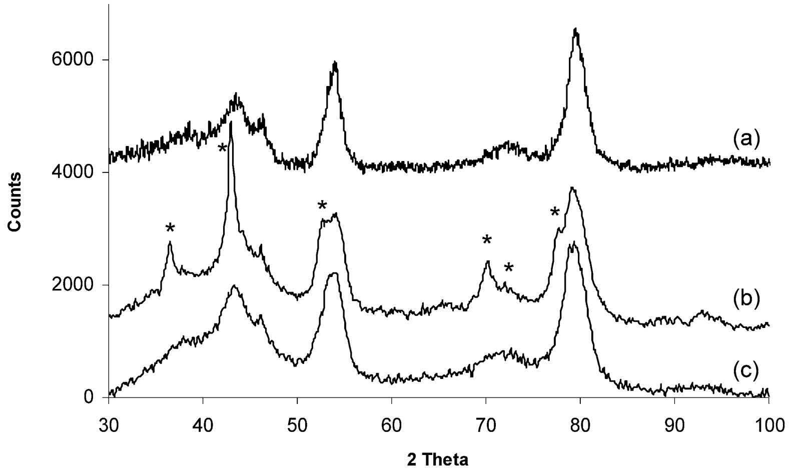

Fig. 11. XRD patterns of samples **1**(c) (line (b)) and **5**(c) (line (c)) and of a γ-Al_2O_3 reference sample (a). Peaks due to Co_3O_4 are marked (∗).

Catalyst **5**(c) combines several features that are beneficial for high catalytic activity in FTS:

- The absence of nitrate ions prevents the formation of large oxidic particles on calcination.
- Using of CO_3^{2-} rather than NO_3^- counter ions in combination with citric acid results in increased pH in the impregnation solution, which enhances the extent of complexation of Co^{2+} by citrate ligands, thereby preventing formation of Co^{2+}-surface complexes on impregnation.
- Migration of the Co precursor into the γ-Al_2O_3 pellets is slow enough to lead to high local Co concentrations near the edge of the support particles (eggshell distribution). Eggshell distributions may reduce CO diffusion restrictions and hence lead to higher reaction rates and higher C_{5+} selectivities in experiments performed under "real" FT conditions, that is, at higher pressures and at higher conversion rates than in the present study [10].
- The presence of Co citrate complexes suppresses redistribution of the catalyst precursor on drying, which restricts the reaction of Co with the support.

4. Conclusion

Changes in the preparation procedure of γ-Al_2O_3-supported Co FT catalysts have a significant effect on the type and size of the Co species present in the resulting catalyst. These different Co–Al_2O_3 species were monitored during all stages of the preparation process using spatially resolved UV–vis microspectroscopy. This study found that the observed catalytic performance of supported Co FT catalysts is the net result of the interaction of Co precursor species with the catalyst support surface, the acidity of the impregnation solution, the nature of the counter anion, and the presence of any complexing agents. These parameters influence the macrodistribution of Co over the support body, the reducibility of the oxidic precursor after calcination, and the dispersion of the metallic particles. The spectroscopic study described here is an example of how analytical tools may aid the development of supported catalysts through monitoring of the preparation process.

Large Co_3O_4 particles, which have only weak interaction with the Al_2O_3 surface, are obtained after calcination when an aqueous $Co(NO_3)_2$ impregnation solution is used for catalyst preparation. The catalytic activity is reasonably good compared with that of the other catalysts investigated due to the good reducibility of large Co_3O_4 crystallites. Using EtOH as the solvent for $Co(NO_3)_2$ impregnation leads to slower Co migration, which ultimately results in an eggshell distribution of Co_3O_4 and some $CoAl_2O_4$ formation by reaction of some of the metal oxide with the support oxide. When $CoCO_3$ is used in combination with citric acid in an aqueous impregnation, a nonhomogeneous, eggshell-type Co distribution is obtained under the preparation conditions studied. The citrate ligands increase the Co dispersion and prevent the formation of $CoAl_2O_4$, which is hard to reduce. Furthermore, an eggshell distribution is observed, because the relatively high pH of the $CoCO_3$/citric acid impregnation solution ensures slow Co migration into the support body. The combination of these factors results in the highest catalytic activity of all samples studied here.

Acknowledgments

B.M.W. acknowledges financial support by the Dutch National Science Foundation (NWO-CW-van der Leeuw and VICI grants) and NRSC-Catalysis.

References

[1] E. Iglesia, Appl. Catal. A Gen. 161 (1997) 59.
[2] H. Schulz, Appl. Catal. A Gen. 186 (1999) 3.
[3] Y.Q. Zhuang, M. Claeys, E. van Steen, Appl. Catal. A Gen. 301 (2006) 138.
[4] A.A. Mirzaei, R. Habibpour, M. Faizi, E. Kashi, Appl. Catal. A Gen. 301 (2006) 272.
[5] F. Morales, F.M.F. de Groot, O.L.J. Gijzeman, A. Mens, O. Stephan, B.M. Weckhuysen, J. Catal. 230 (2005) 301.
[6] F. Morales, D. Grandjean, F.M.F. de Groot, O. Stephan, B.M. Weckhuysen, Phys. Chem. Chem. Phys. 7 (2005) 568.
[7] G.L. Bezemer, U. Falke, A.J. van Dillen, K.P. de Jong, Chem. Commun. (2005) 731.
[8] P.A. Chernavskii, Kinet. Catal. 46 (2005) 634.
[9] J.S. Girardon, A.S. Lermontov, L. Gengembre, P.A. Chernavskii, A. Griboval-Constant, A.Y. Khodakov, J. Catal. 230 (2005) 339.
[10] E. Iglesia, S.L. Soled, J.E. Baumgartner, S.C. Reyes, J. Catal. 153 (1995) 108.
[11] J.A. Bergwerff, L.G.A. van de Water, T. Visser, P. de Peinder, B.R.G. Leliveld, K.P. de Jong, B.M. Weckhuysen, Chem. Eur. J. 11 (2005) 4592.
[12] L.G.A. van de Water, J.A. Bergwerff, B.R.G. Leliveld, B.M. Weckhuysen, K.P. de Jong, J. Phys. Chem. B 109 (2005) 14513.
[13] L.G.A. van de Water, J.A. Bergwerff, T.A. Nijhuis, K.P. de Jong, B.M. Weckhuysen, J. Am. Chem. Soc. 127 (2005) 5024.
[14] A.B.P. Lever, Inorganic Electronic Spectroscopy, second ed., Elsevier, Amsterdam, 1984.
[15] C.M. Lok, S. Bailey, G. Gray, US Patent 6,534,436 (2003).
[16] T. Ataloglou, J. Vakros, K. Bourikas, C. Fountzoula, C. Kordulis, A. Lycourghiotis, Appl. Catal. B Environ. 57 (2005) 299.
[17] C.N.R. Rao, Ultra-Violet and Visible Spectroscopy: Chemical Applications, Butterworths, London, 1967.
[18] J. Vakros, K. Bourikas, S. Perlepes, C. Kordulis, A. Lycourghiotis, Langmuir 20 (2004) 10542.
[19] T. Ataloglou, C. Fountzoula, K. Bourikas, J. Vakros, A. Lycourghiotis, C. Kordulis, Appl. Catal. A Gen. 288 (2005) 1.
[20] J.B.D. De la Caillerie, M. Kermarec, O. Clause, J. Am. Chem. Soc. 117 (1995) 11471.
[21] F. Leroux, E. Moujahid, C. Taviot-Gueho, J.P. Besse, Solid State Sci. 3 (2001) 81.
[22] F. Cavani, F. Trifiro, A. Vaccari, Catal. Today 11 (1991) 173.
[23] A.A. Khassin, V.F. Anufrienko, V.N. Ikorskii, L.M. Plyasova, G.N. Kustova, T.V. Larina, I.Y. Molina, V.N. Parmon, Phys. Chem. Chem. Phys. 4 (2002) 4236.
[24] R. Xu, H.C. Zeng, Chem. Mater. 13 (2001) 297.
[25] S. Morpurgo, M. Lojacono, P. Porta, J. Mater. Chem. 4 (1994) 197.
[26] M. Zayat, D. Levy, Chem. Mater. 12 (2000) 2763.
[27] L.F. Liotta, G. Pantaleo, A. Macaluso, G. Di Carlo, G. Deganello, Appl. Catal. A Gen. 245 (2003) 167.
[28] J. Vakros, C. Kordulis, A. Lycourghiotis, Langmuir 18 (2002) 417.
[29] S. Velu, K. Suzuki, S. Hashimoto, N. Satoh, F. Ohashi, S. Tomura, J. Mater. Chem. 11 (2001) 2049.
[30] B. Jongsomjit, J. Panpranot, J.G. Goodwin, J. Catal. 204 (2001) 98.
[31] J. van de Loosdrecht, M. van der Haar, A.M. van der Kraan, A.J. Van Dillen, J.W. Geus, Appl. Catal. A Gen. 150 (1997) 365.
[32] N. Kotsakis, C.P. Raptopoulou, V. Tangoulis, A. Terzis, J. Giapintzakis, T. Jakusch, T. Kiss, A. Salifoglou, Inorg. Chem. 42 (2003) 22.
[33] A.J. van Dillen, R. Terorde, D.J. Lensveld, J.W. Geus, K.P. de Jong, J. Catal. 216 (2003) 257.